

## Photodesorption of physisorbed hydrogen molecules

M. Hassel, K. Svensson, J. Bellman, S. Andersson, and M. Persson

*Department of Applied Physics, Chalmers University of Technology and Göteborg University, S-412 96 Göteborg, Sweden*

(Received 26 June 2001; revised manuscript received 22 January 2002; published 24 April 2002)

We have determined rates of direct infrared photodesorption for H<sub>2</sub>, HD, and D<sub>2</sub> physisorbed on low-index Cu surfaces. This process relies on the dipole activity of transitions from the ground state to continuum states of the physisorption well. In our calculations a simple functional form for the dipole moment is used, which we find to reproduce accurately the spectroscopically measured dipole intensities for transitions among bound states. The calculated rates of direct desorption, induced by blackbody radiation at different temperatures, agree remarkably well with the measured rates for H<sub>2</sub> adsorbed on the terraces of a Cu(510) surface. A calculated isotope effect on the desorption rate, with a desorption rate for D<sub>2</sub> that is about an order of magnitude smaller than for H<sub>2</sub>, is also in agreement with observations. For HD, the theory predicts the possibility to induce resonant photodesorption by using an infrared laser. We have also found that the calculated rate of photodesorption induced by an indirect process, involving excitation of substrate phonons, is several orders of magnitude smaller than the direct rate.

DOI: 10.1103/PhysRevB.65.205402

PACS number(s): 68.43.Mn, 73.20.Mf, 67.70.+n, 68.43.Pq

### I. INTRODUCTION

Infrared photodesorption of weakly adsorbed species has been observed in a number of experiments,<sup>1-6,11</sup> and different mechanisms have been identified or proposed for the desorption processes. In infrared laser photodesorption experiments, Chuang and Hussla identified desorption following photoexcitation of an internal molecular vibration for NH<sub>3</sub> (Ref. 1) adsorbed on copper. At high laser intensities, thermal desorption due to laser-induced substrate heating was also observed. In an extension of this experiment, with coadsorbed NH<sub>3</sub> and ND<sub>3</sub>, Hussla *et al.*<sup>2</sup> found no molecular selectivity of the desorption when the NH<sub>3</sub> molecules were initially excited. This indiscriminant behavior suggests that the desorption process is thermal. Nonthermal photodesorption was observed in cases where the photon source is blackbody radiation. The interest in this process first arose from observations that were made by Chubb *et al.*,<sup>3</sup> in work that concerned the design of cryopumps. In this study, they found that infrared radiation from the room-temperature walls of the ultrahigh-vacuum (UHV) chamber induced desorption of H<sub>2</sub> from the cryosurface. It was estimated that, without restriction of the thermal radiation load on the cryosurface, the photodesorption could reduce the efficiency of the cryopump substantially. The rate of desorption was found to be independent of the substrate temperature below 4 K, suggesting that the process is nonthermal. In later work,<sup>4</sup> these observations were confirmed for a variety of metallic and nonmetallic surfaces, and it was suggested that the desorption was caused by photon-excited substrate phonons. Further observations of blackbody radiation-induced desorption were made by Cui *et al.*<sup>5</sup> for molecular hydrogen physisorbed on graphite, and by Ferm *et al.*<sup>6</sup> for HD on LiF(100). In the latter case, the measured translational energies of the desorbed molecules were one order of magnitude higher than that given by the substrate temperature, providing direct evidence of the nonthermal nature of the process. The observed photodesorption in these cases was also attributed to the in-

direct mechanism, involving photon-excited substrate phonons.

A direct process, that relies on dipole-excited bound-continuum and bound-bound transitions of the adsorbate in the adsorption well, was also suggested for photodesorption.<sup>7-10</sup> In the case of a chemisorbed molecule such as CO on Cu, Jedrzejek *et al.*<sup>8</sup> found, in a theoretical study based on a one-dimensional, quantum-mechanical model, that this process required a very large photon intensity that cannot be realized by conventional lasers. The specific case of photodesorption of a physisorbed molecule by a bound-continuum transition was theoretically studied by Pearlstine and McClelland.<sup>9</sup> They derived expressions for the rate of direct photodesorption from the ground state to the continuum states of a Morse potential and calculated photodesorption rates using a model for the dipole moment of D<sub>2</sub> physisorbed on LiF(001). A similar theoretical study was performed by Shiang<sup>10</sup> for HF on a LiF(001) surface. However, in these two studies there were no experimental inputs for the dipole activity and no experimental values for photodesorption were available.

In a recent paper,<sup>11</sup> we presented strong evidence of direct photodesorption from the good agreement between measured and calculated photodesorption rates for H<sub>2</sub> and D<sub>2</sub> physisorbed on the terraces of a Cu(510) surface. The experiments showed that molecules desorb due to thermal radiation from the UHV chamber walls, and desorption rates were determined by measuring both the pressure required to maintain a constant surface coverage of adsorbed molecules and the decay of H<sub>2</sub> vibrational spectroscopic intensities with time. From the spectroscopic measurements, dipole activities of transitions in the physisorption well were also observed and intensities for transitions between bound vibrational states were obtained for H<sub>2</sub>, D<sub>2</sub>, and HD. From these data, we have calculated the rate of direct photodesorption, induced by blackbody radiation, and found excellent agreement with the measured desorption rates. We also estimated the contribution from the indirect phonon-mediated process to be negligible.

In this paper, we present in detail the theory and results of our calculations for  $H_2$  and  $D_2$  in Ref. 11, and discuss interesting results for HD which are of particular relevance for possible infrared laser-induced desorption experiments. We derive expressions for the rate of direct photodesorption for two extreme cases of photon sources; a laser beam and blackbody radiation. The direct rate is determined by the dipole intensity spectrum for transitions between the ground state and continuum states of the physisorption well, and we calculate these intensities in the time domain by numerical wave-packet propagation. In these calculations, we use a model for the dipole moment which reproduces accurately measured intensities among bound states of the physisorption well. Calculations of the rate of desorption induced by the indirect process involving excitation of substrate phonons are described and discussed. In this case we also present a simple argument why the photodesorption rate by absorption of a single-photon process dominates over the photodesorption rate for absorption of multiple photons.

The paper is organized as follows. In Sec. II A, we derive expressions for the rate of direct photodesorption by absorption of single photons for the two-photon sources and in Sec. II B we present how the desorption rate from absorption of multiple photons can be calculated. The rate of desorption induced by the indirect process is then derived in Sec. II C. The rate expressions contain spectral functions, which we calculated using a method of wave packet propagation, described in Sec. II D. The propagation takes place on a potential energy surface that is described in Sec. II E. The numerical method of the wave packet propagation is detailed in Appendix B. In Sec. III we describe the experimental procedure and observations. In Sec. IV A, we present a dipole moment function and compare dipole intensities calculated with this function with measured values. The direct rate of photodesorption, calculated with this dipole function, and the indirect rate of photodesorption are presented in Sec. IV B and compared to measured desorption rates. Finally, we give some concluding remarks in Sec. V.

## II. THEORY

### A. Rate of direct infrared photodesorption by absorption of single photons

In this section we present expressions for the photodesorption rate for a hydrogen molecule physisorbed on a low-index metal surface in the low-coverage limit via absorption of single photons. The rates are derived using first-order perturbation theory for two extreme cases of incident photon fields. First we consider a field with a definite frequency, angle of incidence, and polarization, corresponding to a situation with an incident infrared laser beam, and then we consider the case of primary interest here, namely, incident blackbody radiation. We begin by presenting an appropriate Hamiltonian for the molecule-surface interaction and for the interaction of a physisorbed molecule with the electromagnetic field at a metal surface.

In the case of physisorbed  $H_2$  and  $D_2$  molecules on a low-index metal surface, the molecule-surface interaction is relatively simple. Experimental and theoretical studies have

shown that the weak physisorption interaction is essentially electronically adiabatic and is dominated by its laterally and rotationally averaged rigid part, and that the intramolecular vibrational motion is unaffected by the physisorption.<sup>12</sup> For instance, in  $H_2$  and  $D_2$  beam scattering experiments from Cu(100), the behavior of various selective adsorption resonances show that lateral and rotational motions of the physisorbed molecule are essentially unhindered, since the dispersions of these resonances with lateral momentum are free-particle-like, and splittings of rotational sublevels are minute.<sup>13</sup> Thus a good zero-order description of the dynamics of physisorbed  $H_2$  and  $D_2$  molecules is obtained by a Hamiltonian where only the motion of the center-of-mass coordinate  $z$  is hindered by a one-dimensional physisorption potential  $V_0(z)$ . The Hamiltonian  $H_z$  for this motion is then given by

$$H_z = \frac{p_z^2}{2m_p} + V_0(z). \quad (1)$$

The form of  $V_0(z)$  is more or less well characterized for hydrogen molecules adsorbed on several metal surfaces. In a later subsection, we present in detail the form of  $V_0(z)$  for hydrogen molecules physisorbed on Cu(100), as derived from experimental and theoretical studies of selective adsorption resonances.<sup>14</sup>

The electronically adiabatic interaction of HD with the surface is the same as for  $H_2$  and  $D_2$ , but the mass asymmetry of HD introduces a mechanical coupling between the vibrational and rotational motion. For HD, the center of mass  $z$  is displaced by  $d \cos \theta$  from the center of mass for  $H_2$  and  $D_2$ , where  $d = (m_D - m_H)r_0 / (2(m_D + m_H))$  and  $r_0$  is the intermolecular distance and  $\theta$  is the angle between the surface normal and the molecular axis. This asymmetry introduces a coupling between the motion of  $z$  and  $\theta$  through  $V_0(z - d \cos \theta)$ , so that the rotational angular momentum  $J$  is no longer a constant of motion. The interaction is still axially symmetric so  $J_z$  remains conserved. The resulting Hamiltonian for these degrees of freedom for a state with an azimuthal angular momentum  $J_z = \hbar m_j$  is now given by

$$H_{z,\theta} = \frac{p_z^2}{2m_p} - \frac{\hbar^2}{2I} \left[ \frac{1}{\sin \theta} \frac{\partial}{\partial \theta} \left( \sin \theta \frac{\partial}{\partial \theta} \right) - \frac{m_j^2}{\sin^2 \theta} \right] + V_0(z - d \cos \theta), \quad (2)$$

where  $I$  is the moment of inertia of the molecule.

The interaction of an electromagnetic radiation field with a physisorbed molecule is strongly influenced by the presence of the metal surface due to the screening by the conduction electrons. In the physisorption region, which is located well outside the outermost atomic plane, the effect of the screening is described by the reflection coefficients  $R_s$  and  $R_p$  for  $s$ - and  $p$ -polarized incident fields, respectively. The coefficients, given by the Fresnel formulas,<sup>15</sup> are functions of the angle of incidence, and depend on the substrate dielectric properties. Within classical local optics the bulk dielectric function is given by the Drude expression, which for a metal in the infrared spectral range gives a value

$\epsilon \ll -1$ , resulting in almost perfect reflection with  $R_s \approx -1$  and  $R_p \approx 1$ , except at near grazing incidence where  $R_p \rightarrow -1$ . In the present case, a local optics treatment is not valid. For instance, the low temperature of the substrate gives a mean free path of  $\sim 100 \mu\text{m}$  for the conduction electrons, which is larger than the wavelength of  $\sim 40 \mu\text{m}$  for the infrared radiation of interest here. However, the conclusion about the reflectivity from local optics is still valid. For instance, we find that the application of a nonlocal theory to this case gives  $|R_p|^2 \approx 0.997$  at normal incidence.<sup>16</sup>

In the infrared frequency range the response of the metal to an external electric field can be modeled simply using the following two approximations. First the wavelength is much larger than the size of the molecule and the distance between the molecule and the surface, Second, the frequencies in this range are much less than the plasma frequency, so that the response of the conduction electrons is essentially that of a static field. Thus the total electric field in the infrared frequency range at the molecule has a negligible tangential component and a normal component enhanced by a factor of 2. With an incident electromagnetic plane wave with wave vector  $\mathbf{q}$  and polarization  $\boldsymbol{\epsilon}$ , the resulting total electric field at the surface is given by

$$\mathbf{E} = E_z \hat{z} = 2 \hat{z} E(\mathbf{q}, \boldsymbol{\epsilon}) \boldsymbol{\epsilon} \cdot \hat{z} \cos \omega t, \quad (3)$$

where  $E(\mathbf{q}, \boldsymbol{\epsilon})$  is the amplitude of the incident wave,  $\omega = cq$ , and  $\hat{z}$  is the unit normal of the surface. Thus this field couples only to the normal component of the dipole moment of the physisorbed molecule,  $\mu_p$ , resulting in an interaction Hamiltonian  $H_{\text{dip}}$  given by

$$H_{\text{dip}} = -\mu_p E_z. \quad (4)$$

The dipole moment results from the electronic rearrangements associated with the physisorption interaction, and suggests that  $\mu_p$  depends predominantly on  $z$ ,  $\mu_p = \mu_p(z)$ , which enables the perturbation to induce transitions among translational states of the molecule in the physisorption potential by absorption of single photons. A particular consequence of this perturbation is that a molecule may be excited from the ground state to a continuum state resulting in direct photodesorption.

With an incident beam of photons with a definite wave vector  $\mathbf{q}$  and polarization direction  $\boldsymbol{\epsilon}$ , we find that the rate of direct photodesorption by absorption of single photons is given by first order perturbation theory as

$$W_d(\mathbf{q}, \boldsymbol{\epsilon}) = \sigma_d(\mathbf{q}, \boldsymbol{\epsilon}) I(\mathbf{q}, \boldsymbol{\epsilon}), \quad (5)$$

where  $I(\mathbf{q}, \boldsymbol{\epsilon}) = c |E(\mathbf{q}, \boldsymbol{\epsilon})|^2 / 8\pi\hbar\omega$  is the photon flux of the incident beam. At a zero substrate temperature, the cross section  $\sigma_d(\mathbf{q}, \boldsymbol{\epsilon})$  for direct desorption of a single molecule is given by

$$\sigma_d(\mathbf{q}, \boldsymbol{\epsilon}) = \frac{16\pi^2 \omega}{\hbar c} (\boldsymbol{\epsilon} \cdot \hat{z})^2 C_{\mu_p}(\omega), \quad (6)$$

where  $C_{\mu_p}(\omega)$  is the dipole spectral function defined as

$$C_{\mu_p}(\omega) = \sum_m |\langle m | \mu_p | 0 \rangle|^2 \delta(\omega - \omega_m + \omega_0). \quad (7)$$

Here  $|0\rangle$  is the ground state, and in general the sum is over bound and continuum states  $|m\rangle$  of  $V_0(z)$  with energies  $E_m = \hbar\omega_m$ , but only the continuum states of  $V_0(z)$  with  $E_m = \hbar\omega - D > 0$ , where  $D = -E_0$  is the binding energy, contribute to desorption.

There are a few characteristic features of this desorption process. The rate is linear in the photon intensity for  $p$ -polarized light, whereas  $s$ -polarized light gives a negligible contribution. The transition of the molecule is vertical in the physisorption well, with no change of lateral momentum. At a low substrate temperature the molecules have a small lateral momentum and the angular distribution of the desorbed molecules will be sharply peaked in the direction normal to the surface, in sharp contrast to thermally desorbed molecules, which show a broad angular distribution.

In blackbody radiation, the energy flux of photons is the same for all directions  $\hat{q}$  and polarizations  $\boldsymbol{\epsilon}$ . The photon flux within the solid angular element  $d\Omega$ , and with energies in the interval  $\hbar\omega$  to  $\hbar\omega + d(\hbar\omega)$ , is given by  $i(\mathbf{q}, \boldsymbol{\epsilon}) d\omega d\Omega$ , where

$$i(\mathbf{q}, \boldsymbol{\epsilon}) = \frac{n(\omega) \omega^2}{8\pi^3 c^2}. \quad (8)$$

Here  $n(\omega) = [\exp(\hbar\omega/k_B T) - 1]^{-1}$  is the Bose-Einstein distribution function of blackbody radiation photons at a temperature  $T$ . The remaining factors  $c$  and  $\omega^2/8\pi^3 c^3$  are the velocity of light and the photon density of states, respectively. The rate of direct photodesorption is then obtained from Eq. (5) by integrating over the distribution in Eq. (8) for  $p$ -polarized photons with energies  $\hbar\omega > D$  and  $q_z < 0$ , and the result is given by

$$W_d^{\text{th}} = \frac{8}{3\hbar c^3} \int_{\hbar\omega > D} d\omega n(\omega) \omega^3 C_{\mu_p}(\omega). \quad (9)$$

This expression is closely related to the expression for the rate of photon absorption by a dipole in free space. The difference is a factor of 2, arising from the normal electric-field intensity being enhanced by a factor of 4 outside the surface and the total photon irradiation being decreased by a factor of 2.

## B. Photodesorption kinetics and multiple-photon absorption

So far we have considered photodesorption via a bound-continuum state transition by absorption of a single photon. In the presence of a blackbody radiation, we have photons with energies being resonant with bound-bound state transitions in the physisorption well and a photodesorption pathway involving intermediate bound-bound state transitions by absorption of multiple photons is possible. In this subsection we provide the necessary theoretical background and the physical simplifications that can be used to estimate the ef-

efficiency of this process. We also present our procedure to extract the photodesorption rate from the observed rise in the background pressure.

An appropriate theoretical description of the rate of photodesorption by absorption of photons from a surrounding bath of blackbody radiation is provided by the Pauli master equation. The justification and limitations of this approach was discussed by Jedrzejek *et al.*<sup>8</sup> In this description, the time dependence of the rates of population  $P_m$  of the various bound-state levels  $m$  are given by

$$\begin{aligned} \dot{P}_m(t) = & \sum_{m'} (W_{m,m'}^{\text{sub}} + W_{m,m'}^{\text{IR}}) P_{m'}(t) \\ & - \sum_{m'} (W_{d,m'}^{\text{sub}} + W_{d,m'}^{\text{IR}}) P_{m'}(t) \end{aligned} \quad (10)$$

where the off-diagonal matrix elements of the rate matrices,  $W_{m,m'}^{\text{sub}}$  and  $W_{m,m'}^{\text{IR}}$ , give the transition rates among the bound state levels caused by emission and absorption of single substrate phonons, and single photons, respectively.  $W_{d,m'}^{\text{sub}}$  and  $W_{d,m'}^{\text{IR}}$  are the corresponding bound to continuum state transition rates. The diagonal matrix elements of the rate matrices are determined directly by particle conservation from their off-diagonal elements.

In the case of the physisorbed hydrogen molecule on copper, we have a detailed quantitative model for the transition rates that enables us to calculate the desorption rates.  $W_{d,m'}^{\text{IR}}$  is given by Eq. (9), with the dipole spectral function for the bound state  $m$  and the off-diagonal elements of  $W^{\text{IR}}$  are given in analogous manner by

$$W_{m,m'}^{\text{IR}} = \frac{8}{3\hbar c^3} n(\omega_{m,m'}) \omega_{m,m'}^3 |\langle m | \mu_p | m' \rangle|^2, \quad (11)$$

where  $\omega_{m,m'} = (E_m - E_{m'})/\hbar$  is a transition frequency. Note that the emission and absorption processes correspond to negative and positive transition frequencies, respectively [ $n(-\omega) = -(1 + n(\omega))$ ]. In an earlier, combined theoretical and experimental study of lifetimes of physisorbed hydrogen molecules, we showed that they are governed by single-phonon emission and absorption processes, and that at a large lateral parallel momentum the bound-continuum transitions induced by the corrugation of the physisorption potential also give an important contribution to the lifetime.<sup>17</sup> In the case of photodesorption by IR photons with essentially zero momentum and at substrate temperatures below  $\sim 10$  K, states with a large lateral momentum have a negligible population and the latter process is unimportant. Explicit expressions for rates of single-phonon emission and absorption were given in Refs. 17 and 18). They have a structure similar to that of the expressions in Eqs. (9) and (11), but with a different boson density of states and matrix element.

In the specific case of photodesorption of physisorbed hydrogen molecules, we have a few important physical simplifications that make it unnecessary to solve Eq. (11) numerically. At low substrate temperatures, the rate of phonon

absorption is much weaker than the phonon emission. Furthermore, the dipole coupling to the photon field is typically very weak compared to the coupling to the substrate phonons, so that  $W_{d,m'}^{\text{sub}}$  and  $W_{d,m'}^{\text{IR}}$  can be treated by first-order perturbation theory in a similar manner to what was done by Montroll and Shuler.<sup>20</sup> The resulting desorption rate  $R_d$  is then simply given by

$$R_d = \sum_m (W_{d,m}^{\text{sub}} + W_{d,m}^{\text{IR}}) P_{\text{quasi},m}, \quad (12)$$

$$\sum_{m'} (W_{m,m'}^{\text{sub}} + W_{m,m'}^{\text{IR}}) P_{\text{quasi},m'} = 0, \quad (13)$$

where  $P_{\text{quasi},m}$  is the stationary population of the bound-state levels in the absence of bound-to-continuum-state transitions. Furthermore, the weak coupling to the photons relative to the substrate phonons also makes it possible to treat the effect of single-photon emission and absorption on  $P_{\text{quasi}}$  by perturbation theory, and the first-order change  $P_{\text{quasi}}^{(1)}$  is determined by

$$W^{\text{sub}} P_{\text{quasi}}^{(1)} = -W^{\text{IR}} P_{\text{quasi}}^{(0)}, \quad (14)$$

where  $P_{\text{quasi}}^{(0)}$  is the stationary population in the absence of blackbody radiation and bound-to-continuum state transitions. The component of  $P_{\text{quasi}}^{(1)}$  that is linearly dependent on  $P_{\text{quasi}}^{(0)}$  is indeterminate from Eq. (14), but is determined from particle conservation. In particular, at zero substrate temperature,  $P_{\text{quasi},m}^{(0)} = \delta_{m,0}$  and  $P_{\text{quasi},m}^{(1)}$ , with  $m > 0$ , reduce to

$$P_{\text{quasi},m}^{(1)} = \frac{W_{m,0}^{\text{IR}}}{\Gamma_{m,m}^{\text{sub}}} + \frac{1}{\Gamma_{m,m}^{\text{sub}}} \sum_{k=1}^{\infty} \{ [W_{OD}^{\text{sub}} (\Gamma^{\text{sub}})^{-1}]^k W_{m,0}^{\text{IR}} \}, \quad (15)$$

where  $\Gamma^{\text{sub}}$  is a diagonal matrix acting on all bound states except the ground state,  $m=0$ , whose diagonal elements  $\Gamma_{m,m}^{\text{sub}} = -W_{m,m}^{\text{sub}}$  are the relaxation rates of the bound states due to the interaction with the substrate, and  $W_{OD}^{\text{sub}} = W^{\text{sub}} + \Gamma^{\text{sub}}$ . Finally, using Eqs. (13) and (14), the total desorption rate can now be expressed in a physical transparent form as

$$R_d = R_d^{\text{th}} + R_d^{\text{IR}}, \quad (16)$$

$$R_d^{\text{IR}} = R_d^{\text{IR},(1)} + W_d^{\text{sub}} P_{\text{quasi}}^{(1)} + W_d^{\text{IR}} P_{\text{quasi}}^{(1)}, \quad (17)$$

where  $R_d^{\text{th}} = W^{\text{sub}} P_{\text{quasi},m}^{(0)}$  is the thermal desorption rate in absence of blackbody radiation and  $R_d^{\text{IR}} = W^{\text{IR}} P_{\text{quasi},m}^{(0)}$  is the photodesorption rate induced by blackbody radiation. In Sec. IV B, we will show that  $R_d^{\text{IR}}$  is dominated by the photodesorption rate  $R_d^{\text{IR},(1)}$  via bound-to-continuum-state transitions by absorption of single photons and, in particular, that the two-photon desorption rate  $W_d^{\text{IR}} P_{\text{quasi}}^{(1)}$  is negligible.

Finally, the thermal and the photodesorption rates for single molecules are simply related to measurable quantities, such as the background pressure that is required to maintain a constant coverage of adsorbed molecules. For instance, in an equilibrium situation with a constant surface coverage of

$\Theta$  molecules per unit surface, the rate of incident molecules that stick to the surface is equal to the rate of desorbing molecules:

$$s\Phi = R_d\Theta. \quad (18)$$

Here  $\Phi = p/\sqrt{2\pi m_p k_B T}$  is the flux of incident molecules at a pressure  $p$  and  $s$  is the sticking coefficient. To maintain a specific surface coverage in the presence of photodesorption, it is just necessary to increase the pressure by  $\Delta p_b$  from the background pressure in the absence of radiation where

$$\Delta p_b = \frac{\sqrt{2\pi m_p k_B T}}{s} R_d^{IR}\Theta. \quad (19)$$

### C. Rate of indirect photodesorption

This subsection deals with desorption induced by an indirect process; the field interacts with the dipole moment  $\mu_l$  of the surface substrate ions, and excites substrate phonons, which may decay by transferring energy to the translational motion of the molecule. We first present the rate of substrate phonon excitation by single-photon absorption, and then derive the rate of desorption of a single molecule using second-order perturbation theory.

Our treatment relies on previous studies<sup>19,21</sup> based on electron-energy-loss spectroscopy measurements of the dipole activity of substrate phonons in the surface region of a metal. These studies showed, in particular, that the observed dipole activity of the phonons at the Cu(100) surface is well represented by a surface lattice dipole moment per surface unit cell, given by

$$\mu_l = e^*(u_0 - u_1), \quad (20)$$

where  $e^*$  is the screened charge of the ions and  $u_0$  and  $u_1$  are rigid displacements of the first and second layer, normal to the surface. Thus only longitudinal phonons, propagating in a direction normal to the surface, will be excited. The rate  $w_{\text{ph}}$  of excitation of substrate phonons, per surface unit cell by absorption of single photons with  $\hbar\omega > D$ , is then given by the expressions for dipole excitation in Eqs. (5) and (9) when making the substitution  $\mu_p \rightarrow \mu_l$ . Here,  $C_{\mu_l}(\omega)$  is simply determined from linear-response theory as

$$C_{\mu_l}(\omega) = \frac{\hbar}{\pi} \text{Im} \alpha(\omega), \quad (21)$$

where  $\alpha(\omega) = \mu_l(\omega)/E_z(\omega)$  is the polarizability of the lattice in the surface region. For the Cu(100) surface, a good representation of the surface polarizability is obtained from a simple nearest-neighboring interlayer force-constant model.<sup>19</sup> As shown in the Appendixes, the imaginary part of  $\alpha(\omega)$ , which is related to the power absorbed by the surface, is then given by

$$\text{Im} \alpha(\omega) = \frac{32e^{*2}}{M\omega_{\text{max}}^2} \bar{\omega}^3 \sqrt{1 - \bar{\omega}^2} \quad (22)$$

for  $0 < \bar{\omega} = \omega/\omega_{\text{max}} < 1$ , where  $\omega_{\text{max}}$  is the maximum longitudinal phonon frequency in the [100] direction.

Some of the excited phonons will cause desorption of the adsorbed molecules. A proper treatment of this desorption rate is provided by second-order perturbation theory, which includes both real and virtual intermediate phonon processes. The interaction between longitudinal phonons, propagating in a direction normal to the surface, and a single molecule, via the physisorption potential, is well represented by

$$H_{p-l} = -u_0 V'_0(z). \quad (23)$$

The corresponding second-order expression for the rate of desorption is derived in the Appendixes, and we find that the indirect rate, in terms of the incident photon energy flux, is given by

$$W_{\text{ph}}(\mathbf{q}, \boldsymbol{\epsilon}) = \frac{16\pi^2 \omega I(\mathbf{q}, \boldsymbol{\epsilon})}{\hbar c} (\boldsymbol{\epsilon} \cdot \hat{z})^2 C_{V'_0}(\omega) |\eta(\omega)|^2. \quad (24)$$

Here  $C_{V'_0}(\omega)$  is the force,  $-V'_0$ , spectral function, defined in an analogous manner to the dipole spectral function in Eq. (7), and  $\eta(\omega) = u_0(\omega)/E_z(\omega)$  is the linear response of  $u_0$  to the incident field. The contributions from real and virtual phonons are given by the imaginary and real parts of  $\eta(\omega)$ , respectively. In our lattice-dynamics model of Cu(100),  $|\eta(\omega)|^2$  is given by

$$|\eta(\omega)|^2 = \frac{16e^{*2}}{M^2 \omega_{\text{max}}^4} \quad (25)$$

for  $0 < \omega < \omega_{\text{max}}$ .

The contribution from  $|\text{Im} \eta(\omega)|^2$  to the rate in Eq. (24) can be interpreted as a two-step process. This interpretation is based on the factorization

$$W_{\text{ph}}^{\text{real}}(\mathbf{q}, \boldsymbol{\epsilon}) = \sigma_{\text{ph}}(\omega) P_{\text{abs}}(\mathbf{q}, \boldsymbol{\epsilon}) I(\mathbf{q}, \boldsymbol{\epsilon}), \quad (26)$$

where

$$P_{\text{abs}}(\mathbf{q}, \boldsymbol{\epsilon}) = \frac{w_{\text{ph}}(\mathbf{q}, \boldsymbol{\epsilon})}{A_{\text{sc}} I(\mathbf{q}, \boldsymbol{\epsilon})} = \frac{512\pi e^{*2}}{Mc\omega_{\text{max}} A_{\text{sc}}} (\boldsymbol{\epsilon} \cdot \hat{z})^2 \bar{\omega}^4 \sqrt{1 - \bar{\omega}^2} \quad (27)$$

and

$$\sigma_{\text{ph}}(\omega) = \frac{W_{\text{ph}}^{\text{real}}(\mathbf{q}, \boldsymbol{\epsilon})}{w_{\text{ph}}(\mathbf{q}, \boldsymbol{\epsilon})} A_{\text{sc}} = \frac{2\pi}{M\hbar\omega_{\text{max}}^2} \frac{\sqrt{1 - \bar{\omega}^2} C_{V'_0}(\omega)}{\bar{\omega}} A_{\text{sc}} \quad (28)$$

for  $D < \hbar\omega < \hbar\omega_{\text{max}}$ . Here  $A_{\text{sc}}$  is the area of the surface unit cell. The factor  $P_{\text{abs}}(\mathbf{q}, \boldsymbol{\epsilon})$  is the probability for a photon to be absorbed by a longitudinal phonon with energy  $\hbar\omega = c\hbar q$ . The factor  $\sigma_{\text{ph}}(\omega)$  is then the cross section for such a phonon to desorb the molecule.

### D. Spectral functions

The basic quantities in the expressions [Eqs. (5) and (24)] for the desorption rates that we need to calculate are the spectral functions  $C_F(\omega)$ , where  $F = \mu_p$  and  $F = V'_0$ , respec-

tively. In the case of HD, we had to calculate these spectral functions for a two-dimensional potential,  $V_0[z - d \cos(\theta)]$ , so we chose to calculate these functions using a wave-packet propagation method.<sup>22</sup> We also applied this method to H<sub>2</sub> and D<sub>2</sub> where we only had to propagate a wave packet in the one-dimensional potential  $V_0(z)$ . This method is based on the time evolution of an autocorrelation function, and, in the time domain, the spectral function of  $F$  is directly related to such a correlation function through

$$C_F(t) = \sum_m e^{-i(\omega_m - \omega_0)t} \langle m|F|0 \rangle^2 = \langle 0|F(t)F(0)|0 \rangle. \quad (29)$$

Here we have made an expansion in the energy eigenstates of the physisorption potential. However, since the correlation function can only be calculated for a finite-time interval, we weight  $C_F(t)$  with a window function  $W(t)$  before taking the real part of the Fourier transform:

$$\begin{aligned} C_F(\omega) &= \frac{1}{2\pi} \text{Re} \int_0^T dt e^{i\omega t} W(t) C_F(t) \\ &= \sum_m |\langle m|F|0 \rangle|^2 \text{Re} W[\omega - (\omega_m - \omega_0)]. \end{aligned} \quad (30)$$

The real part of the Fourier transform of the window function,  $\text{Re} W(\omega)$ , is peaked at  $\omega=0$  with a width proportional to  $1/T$  and with an integrated strength of unity. Thus, for transitions among bound states,  $C_F(\omega)$  will be peaked at the transition energies,  $\hbar(\omega_m - \omega_0)$ , and the intensity of a specific transition is now determined by integrating  $C_F(\omega)$  over the corresponding peak when  $T$  is chosen large enough so that the peaks from the surrounding bound states do not overlap.

The time evolution of the correlation function in Eq. (29) can be determined by propagating an appropriate wave packet  $|\psi(t)\rangle$  in the physisorption well with the Hamiltonian  $H$  in either Eq. (1) or (2). With  $|\psi(t)\rangle$  given by

$$|\psi(t)\rangle = \exp\left(-\frac{i}{\hbar} H t\right) F|0\rangle, \quad (31)$$

the correlation function can be written in terms of a wave-function autocorrelation function:

$$C_F(t) = \exp\left(\frac{i}{\hbar} E_0 t\right) \langle \psi(t) | \psi(0) \rangle. \quad (32)$$

In the calculation of  $C_F(t)$ , we first need to determine the ground state,  $|\psi(0)\rangle = |0_p\rangle$ . A well-established method<sup>23</sup> to calculate  $|0_p\rangle$  involves the propagation of an initial state that has a nonzero overlap with  $|0_p\rangle$ , in imaginary time  $t = i\tau$ :

$$|\phi(i\tau)\rangle = \exp\left(-\frac{1}{\hbar} (H - E_0)\tau\right) |\phi(0)\rangle. \quad (33)$$

The overlaps of  $|\phi(i\tau)\rangle$  with all states except the ground state will then decay exponentially in time. The expressions in Eqs. (31) and (33) also include the ground-state energy of the system. We have determined the eigenenergies by propa-

gating the wave packet,  $|\phi(0)\rangle$  and calculating the wave-function autocorrelation function in an analogous manner to the calculation of the auto correlation function in Eq. (29). In Appendix B we describe in detail the numerical method that we used for the wave-packet propagation, but first we present the detailed form of the physisorption potential under consideration here; hydrogen molecules physisorbed on a Cu(100) surface.

### E. Physisorption potential

The laterally and rotationally averaged part of the potential,  $V_0(z)$ , is governed by Pauli repulsion close to the surface, while asymptotically it is governed by van der Waals attraction. In current theoretical descriptions of physisorption,<sup>24–26</sup>  $V_0(z)$  is written as a sum of these two branches,

$$V_0(z) = V_R(z) + V_{\text{vdW}}(z), \quad (34)$$

where the repulsive and attractive terms are given by

$$V_R(z) = C_R \exp(-\alpha z) \quad (35)$$

and

$$V_{\text{vdW}}(z) = -C_{\text{vdW}} \frac{f_2[2k_c(z - z_{\text{vdW}})]}{(z - z_{\text{vdW}})^3}, \quad (36)$$

respectively. Here  $C_R$  describes the strength and  $\alpha$  the inverse range of the repulsive potential,  $C_{\text{vdW}}$  is the strength of the van der Waals attraction,  $k_c$  is related to the inverse size of the molecule, and  $z_{\text{vdW}}$  is the position of the van der Waals plane. The saturation of the attraction at short distances is described by  $f_2(x)$ , which is given by

$$f_2(x) = 1 - \left(1 + x + \frac{x^2}{2}\right) e^{-x}. \quad (37)$$

In the present case of a Cu(100) surface, we have used parameters taken from Ref. 13:  $C_R = 5.21$  eV,  $\alpha = 1.21a_0^{-1}$ ,  $C_{\text{vdW}} = 4.74$  eV  $a_0^3$ ,  $k_c = 0.45a_0^{-1}$ , and  $z_{\text{vdW}} = 0.563a_0$ . With these values, the resulting bound state levels of H<sub>2</sub> and D<sub>2</sub> agree well with results from selective adsorption measurements. The shape of  $V_0(z)$  is shown in Fig. 1. Electron-energy-loss spectra taken for H<sub>2</sub> adsorbed on the (100)-like terraces of a Cu(510) surface, (discussed in Sec. III), show that the vibrational energies, defined henceforth as the transition energies between the ground state to excited states of  $V_0(z)$ , practically coincide with those for the flat Cu(100) surface. Hence the molecules in these two cases experience similar potentials, which justifies also using the well-characterized Cu(100) potential in calculations for molecules adsorbed on a Cu(510) terrace.

The isotopic molecules H<sub>2</sub>, HD, and D<sub>2</sub> have the same electronic configurations and thus the same physisorption interaction. However, for HD the asymmetric position of the center of mass introduces a coupling between rotational and vibrational motion [see Eq. (2)], and we find that in order to account quantitatively for observed dipole moment intensities for transitions to rotational states of this molecule, it is

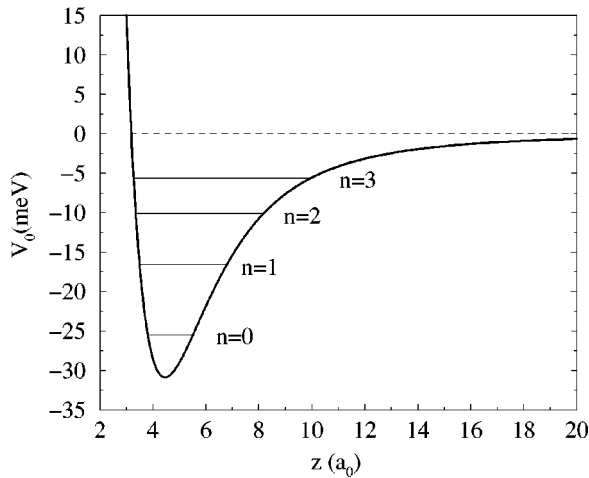


FIG. 1. The isotropic part  $V_0$  of the interaction potential for hydrogen molecules physisorbed on Cu(100). The energies of the lowest bound states for  $H_2$  are indicated.

necessary to include the anisotropy of the potential, that is, its dependence on the angle,  $\theta$ , between the surface normal and the molecular axis. Current theory and the observed splittings (see Sec. III) of the bound-state levels suggest that the anisotropy is well described by the leading-order anisotropic term in an expansion of  $V(z, \theta)$  in Legendre functions:

$$V(z, \theta) = V_0(z) + V_2(z)P_2(\cos \theta). \quad (38)$$

The anisotropic term  $V_2(z)$  is written as a linear combination of the repulsive and attractive parts of  $V_0(z)$ :

$$V_2(z) = \beta_R V_R(z) + \beta_{vdW} V_{vdW}(z). \quad (39)$$

The anisotropy of the van der Waals attraction was calculated previously<sup>27</sup> giving  $\beta_{vdW} = 0.05$ . With this value and with  $\beta_R = -0.002$ , both the magnitudes and signs of the splittings are reproduced.<sup>13</sup> Note that the anisotropy is dominated by the attractive part.

### III. EXPERIMENT

In this section, we describe experiments that measure rates of desorption of  $H_2$  and  $D_2$  caused by background blackbody radiation. We have used two different methods to determine the desorption rates. One method relies on vibrational loss intensity measurements using high-resolution electron-energy-loss spectroscopy (EELS) and the other on retarding field measurements of the adsorbate-induced work-function change.<sup>11</sup> The latter measurements were performed in a small side chamber, whose wall temperature could be varied during the experiments. This chamber is directly attached to the main ultrahigh-vacuum system which operates at a base pressure in the  $10^{-11}$  Torr range.

The x-ray-aligned ( $<0.2^\circ$ ) and -polished Cu(510) specimen was cleaned *in situ* by standard procedures involving low-energy argon-ion bombardment and heating cycles. Using helium as a cryogen, the specimen could be cooled to below 10 K, and it was heated resistively. Substrate surface properties were monitored by low-energy electron diffraction

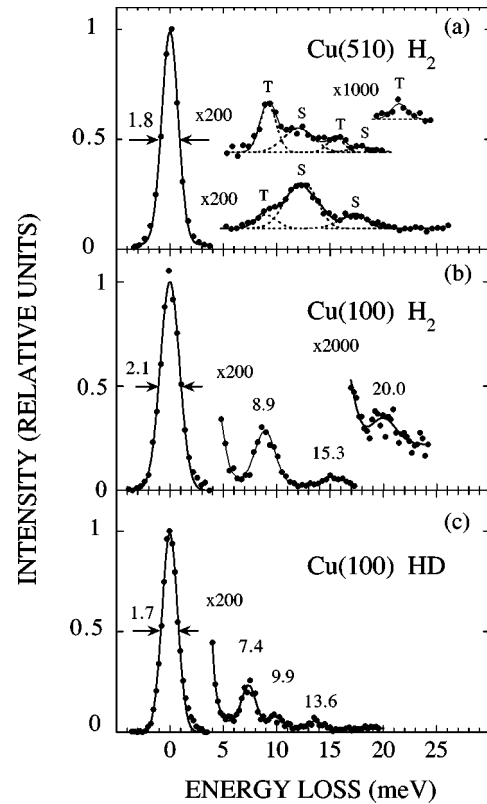


FIG. 2. (a) displays electron-energy-loss spectra for  $H_2$  adsorbed on Cu(510) at 9 K for initial gas exposures of 0.7 L (lower curve) and 1.6 L (upper curve), where  $1 \text{ L} = 1 \times 10^{-6} \text{ Torr sec}$ . A smooth background has been subtracted, and the dashed curves indicate decomposition in step (S) and terrace (T) related features. (b) and (c) show spectra for full monolayers of  $H_2$  and HD, respectively, adsorbed on Cu(100) at 10 K. All spectra are measured in the specular direction at a  $48^\circ$  angle of incidence relative to the surface normal. The electron-beam energies were 1 eV [Cu(510)] and 3 eV [Cu(100)], respectively.

(LEED) and high-resolution EELS, measurements. The clean Cu(510) surface exhibited the expected LEED pattern, with split diffraction spots in the  $[5\bar{1}0]$  direction, corresponding to an average surface topology with (100)-like terraces that are five atomic rows wide and separated by (110)-like steps. Prior to hydrogen adsorption, the specimen was flash heated to 900 K and rapidly cooled ( $<3$  min) to 10 K. The hydrogen adsorption was monitored by mass spectroscopy, work-function measurements, and high-resolution EELS. The latter measurements were obtained with use of an electron spectrometer which is a modified version of a construction that was described elsewhere,<sup>28</sup> and has an optimum energy resolution of about 1 meV.

The electron-energy-loss measurements show that hydrogen molecules adsorb on Cu(510) at low temperature (around 10 K) in two characteristic stages; the steps are occupied first and further adsorption populates the terraces.<sup>11</sup> Figure 2 illustrates this behavior in a series of EEL spectra obtained for specular electron scattering; (a) from Cu(510), and (b) and (c) from Cu(100). In (a) lower curve primarily the steps (S) are covered and in the upper curve both steps (S) and terraces (T) are covered with adsorbed  $H_2$ . The loss

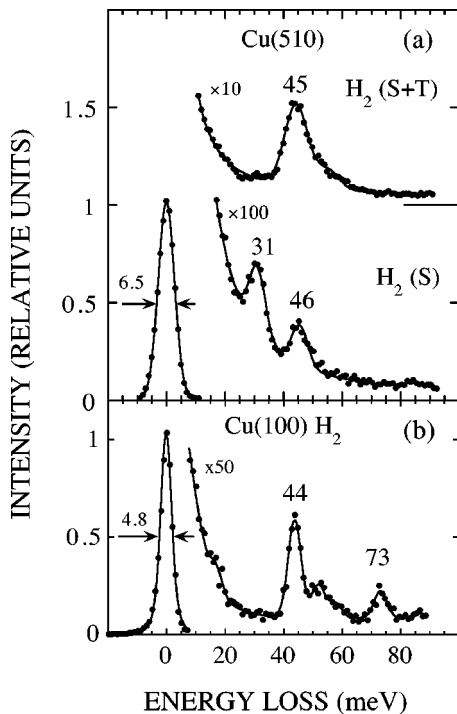


FIG. 3. (a) displays electron-energy-loss spectra for  $H_2$  adsorbed on Cu(510) at 10 K; in the lower curve, only the steps are covered; in the upper curve, both steps and terraces are covered. (b) shows a spectrum for a full monolayer of  $H_2$  on Cu(100) at 10 K. The spectra were measured at  $54^\circ$  detection angle for an angle of incidence of  $48^\circ$  from the surface normal and a 3-eV incident electron energy.

peaks at 9.0, 15.4, and 21.3 meV in the upper curve are due to  $H_2$  adsorbed on the (100)-like terraces. These peaks almost coincide with the  $0 \rightarrow 1$ ,  $0 \rightarrow 2$ , and  $0 \rightarrow 3$  vibrational transitions observed at 8.9, 15.3, and 20.0 meV in (b) for  $H_2$  adsorbed on Cu(100). Evidently, terrace adsorption closely resembles hydrogen physisorption on a flat Cu(100) surface. All of the vibrational excitations observed in Fig. 2 are dipole excited, and the intense overtone excitations are caused by a strongly nonlinear dipole moment function.<sup>29</sup> We also note that the energy of the dipole-active  $0 \rightarrow 3$  transition for  $H_2$  adsorbed on Cu(100) is quite close to the continuum limit around 25 meV. The intensities of the  $0 \rightarrow 1$ ,  $0 \rightarrow 2$ , and  $0 \rightarrow 3$  vibrational transitions provide direct experimental information about the dipole moment function for the  $H_2$  adsorbed on Cu(100) and the terraces of Cu(510).

EELS spectra recorded in the energy range for rotational transitions of adsorbed  $H_2$  reveal a striking difference between step and terrace-adsorbed molecules on Cu(510), as shown in Fig. 3. Molecules adsorbed on the terraces of Cu(510) and on Cu(100) are found to rotate as weakly perturbed three-dimensional (3D) rotors, a characteristic feature of  $H_2$  physisorption on flat crystal surfaces. For dense monolayers of  $H_2$  the  $j=0 \rightarrow 2$  rotational transition is observed around 45 meV for Cu(510) [see Fig. 3(a), upper curve] and at 43.5 meV for Cu(100) [see Fig. 3(b)] that is close to the gas-phase value 44.1 meV.<sup>30,31</sup> The lower spectrum in Fig. 3(a) shows that step-adsorbed molecules exhibit exciting

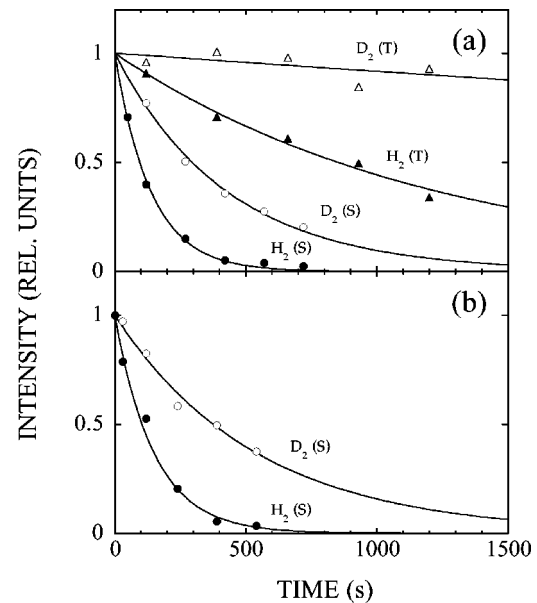


FIG. 4. (a) decay of the  $0 \rightarrow 1$  vibrational peak intensity with time at a background temperature of 296 K for  $H_2$ ( $D_2$ ) adsorbates on Cu(510). *S* and *T* denote step and terrace adsorbed molecules, respectively, and the solid curves represent fitted exponential decays. (b) Corresponding data for an equal mixture of step-adsorbed  $H_2$  and  $D_2$ .

properties;  $H_2$  is adsorbed in two rotor states resembling 2D and 3D rotors. We suggest that the 3D rotor state corresponds to terrace adsorption at the lower step edge, where the molecule experiences attraction to both the terrace and the step edge. Density-functional calculations<sup>32</sup> showed that the 2D rotor state corresponds to  $H_2$  weakly bonded to a copper atom at the step edge.

Desorption of  $H_2$  due to background blackbody radiation is a pronounced effect for  $H_2$  adsorbed on Cu(510), and we obtained the spectra by applying an  $H_2$  pressure in order to maintain a fixed  $H_2$  coverage. With the vacuum chamber at room temperature (296 K), a pressure of  $4 \times 10^{-9}$  Torr is required to keep the steps, for example, saturated with adsorbed  $H_2$ . This pressure is independent of substrate temperature below 13 K, but depends on the temperature of the surrounding wall of the vacuum chamber. At a wall temperature of 240 K the applied pressure required is about a factor of 2 lower. The specimen temperature is unaffected by the changing radiation load. These observations are consistent with related findings for a number of  $H_2$  physisorption systems,<sup>3-6</sup> the desorption is evidently nonthermal, and is induced by the infrared radiation emitted from the walls.

Both step- and terrace-adsorbed molecules on Cu(510) are desorbed by the thermal radiation. We have determined desorption rates for both kinds of molecules by simply measuring the decay of the  $0 \rightarrow 1$  vibrational peak intensity with time. It is straightforward to use this method for step-adsorbed molecules, and such measurements with the vacuum chamber at room temperature are shown in Fig. 4(a). The initial gas exposures were 0.5 and 1.0 L (1 L =  $1 \times 10^{-6}$  Torr sec) for  $H_2$  and  $D_2$ , respectively. The influence of a low residual  $H_2$  ( $D_2$ ) pressure has been corrected for.

TABLE I. Dipole moment matrix elements  $|\langle n,j|\mu|0,0\rangle|$  for hydrogen molecules physisorbed on Cu(100). Values (a) were calculated using the dipole moment function in Eq. (40) with  $\beta=0.9a_0^{-1}$  and  $\mu_0=0.051$  D. Values (b) were calculated using a linear dipole moment function;  $\mu=\mu_0-\mu_1(z-z_0)$ , where  $\mu_0=0.0553$  D,  $\mu_1=0.0330$  D, and  $z_0$  is the position of the potential energy minimum.  $n$  and  $j$  denote vibrational and rotational quantum numbers, respectively. The unit is Debye.

$n,j$	$H_2$				$HD$		$D_2$	
	Expt. <sup>a</sup>	Calc. <sup>a</sup>	Calc. <sup>(a)</sup>	Calc. <sup>(b)</sup>	Expt. <sup>a</sup>	Calc. <sup>(a)</sup>	Expt. <sup>a</sup>	Calc. <sup>(a)</sup>
0,0	0.045	0.026	0.045	0.045				0.047
1,0	0.020	0.016	0.020	0.020	0.018	0.017	0.017	0.018
2,0	0.009	0.006	0.010	0.005	0.008	0.010	0.007	0.009
0,1					0.008	0.007		
3,0	0.005		0.006	0.002			0.004	0.005
4,0			0.004	0.001				0.003

<sup>a</sup>Reference 29; the experimental  $n,j=3,0$  values for  $H_2$  and  $D_2$  were obtained in the present work.

The intensity decays in an exponential fashion with time,  $I(t)=I_0 \exp(-t/\tau)$ , where  $\tau$  is the mean lifetime of an adsorbed molecule. We obtain desorption rates  $1/\tau$ , of  $7 \times 10^{-3} \text{ s}^{-1}$  for  $H_2$  and  $2 \times 10^{-3}$  for  $D_2$ . Terrace-adsorbed molecules diffuse easily to unoccupied step sites and photo-desorb. This means that desorption rates for such molecules are not readily measured from spectra like the upper curve in Figs. 2(a).  $H_2$  adsorption at the steps can be prevented, however, via preadsorption of a suitable inert adsorbate. We found that  $N_2$  serves this purpose well;<sup>33</sup> the molecules adsorb stably at the steps, prevent step adsorption of  $H_2$ , and affect the subsequent  $H_2$  adsorption on the terraces only marginally as judged from the EEL spectra. The fundamental  $0 \rightarrow 1$  vibrational transition in the physisorption well is observed at around 9 and 7 meV for  $H_2$  and  $D_2$ , respectively. The loss peak intensity decays with a long time constant, as can be seen in Fig. 4(a). The corresponding desorption rate is  $8 \times 10^{-4} \text{ s}^{-1}$  for  $H_2$ , and about an order of magnitude lower for  $D_2$ . Our measurements do not permit a more precise determination for  $D_2$  because of influence from the ambient gas. The larger rates measured for step-adsorbed  $H_2$  and  $D_2$  relate qualitatively to a large dipole activity of the vibrational motion.

We also performed measurements for step-adsorbed molecules with an equal mixture of  $H_2$  and  $D_2$ . The decay of the  $0 \rightarrow 1$  vibrational peak intensities with time is displayed in Fig. 4(b). The desorption rates are  $7 \times 10^{-3}$  and  $2 \times 10^{-3} \text{ s}^{-1}$  for  $H_2$  and  $D_2$ , respectively, that is precisely the same values as we measured for the pure  $H_2$  and  $D_2$  layers. The desorption rates are clearly independent of the isotopic composition of the adsorbate layer; an observation that is entirely compatible with a direct photodesorption process.

Desorption rates were also determined using the work-function change to monitor the coverage of adsorbed hydrogen. We have performed such measurements at different background temperatures in the small side chamber. These data were thoroughly discussed in Ref. 11, and we just summarize the observations here. For step-adsorbed molecules and the chamber at room temperature, we find rates of  $8 \times 10^{-3}$  and  $2 \times 10^{-3} \text{ s}^{-1}$  for  $H_2$  and  $D_2$ , respectively, values that agree very well with the corresponding rates obtained from the spectroscopic measurements discussed above. For terrace-adsorbed  $H_2$  we obtain the rate 8

$\times 10^{-4} \text{ s}^{-1}$  with the chamber at room temperature, confirming the rate we measured from the decay of the  $0 \rightarrow 1$  vibrational intensity. The rate decrease to  $5 \times 10^{-4} \text{ s}^{-1}$  when the background temperature is lowered to 210 K, and increases to  $15 \times 10^{-4} \text{ s}^{-1}$  at a temperature of 470 K. The desorption rate for terrace-adsorbed  $D_2$  was so low that we were unable to measure it with this method.

#### IV. RESULTS AND DISCUSSION

The calculation of the photodesorption rates for hydrogen molecules physisorbed on Cu requires a detailed knowledge of the physisorption interaction and the dipole moment function. The form of this interaction is well-characterized, as already discussed in Sec. II E, while our knowledge of the form of the dipole moment function is much less well developed. Here we show that it is possible to construct a simple dipole moment function that reproduces the measured dynamic dipole moments for various transitions of  $H_2$ , HD, and  $D_2$  molecules physisorbed on Cu(100), and also for  $H_2$  molecules physisorbed on the (100)-like terraces of the stepped Cu(510) surface. Using this dipole moment function, we calculate the direct and indirect photodesorption rates for these two physisorption systems, and make a direct comparison with the measured rates for terrace-adsorbed  $H_2$  and  $D_2$  discussed in Sec. III.

##### A. Dipole activity

At the current level of physisorption theory, it is not clear how to calculate the dipole moment function for a physisorbed molecule in the spatial region of interest, where we have comparable contributions from both Pauli repulsion and van der Waals attraction. Therefore, we have resorted to a simple phenomenological model. We find that the measured dynamic dipole moments for hydrogen molecules adsorbed on Cu can be accurately reproduced using a dipole moment function, which is exponentially decreasing outside the surface:

$$\mu_p = \mu_0 e^{-\beta(z-z_0)}. \quad (40)$$

Here  $z_0$  is the position of the potential minimum. Our motivation for this functional form is that the overlap between a

TABLE II. Dipole moment matrix elements  $|\langle n|\mu|0\rangle|$  for  $\text{H}_2$  physisorbed on the terraces of  $\text{Cu}(510)$ . Measured values are taken from Ref. 11 and our values were calculated using the dipole moment function in Eq. (40) with  $\beta=1.5a_0^{-1}$  and  $\mu_0=0.0342$  D.  $n$  denotes the vibrational quantum number. The unit is Debye.

$n$	Calc.	Expt.
0	0.032	
1	0.021	0.021
2	0.014	0.015
3	0.009	0.009
4	0.006	

molecular orbital and the tail of a metal electron wavefunction decreases exponentially with  $z$ . This model reproduces very well the measured dipole moment matrix elements, as demonstrated in Tables I and II for  $\text{H}_2$ , HD, and  $\text{D}_2$  physisorbed on  $\text{Cu}(100)$  and for  $\text{H}_2$  on the terraces of  $\text{Cu}(510)$ , respectively. For both surfaces, the results were obtained by adjusting the parameters  $\mu_0$  and  $\beta$ , so that the calculation reproduces two of the measured dipole moment matrix elements  $|\langle n|\mu|0\rangle|$  for  $\text{H}_2$ . In the former case, this adjustment was done for  $n=0$  and 1, and in the latter case for  $n=1$  and 3. As shown in Tables I and II, we find that our predicted values for the matrix elements for other transitions are in good agreement with all measured values. This kind of agreement makes us confident that the model is appropriate for calculating direct desorption rates that involve transitions to the continuum.

In Figs. 5 and 6, we show the calculated dipole spectral functions  $C_{\mu_p}(\omega)$  for  $\text{H}_2$  and  $\text{D}_2$ , respectively, adsorbed on  $\text{Cu}(100)$ . Each spectrum consists of two distinct energy re-

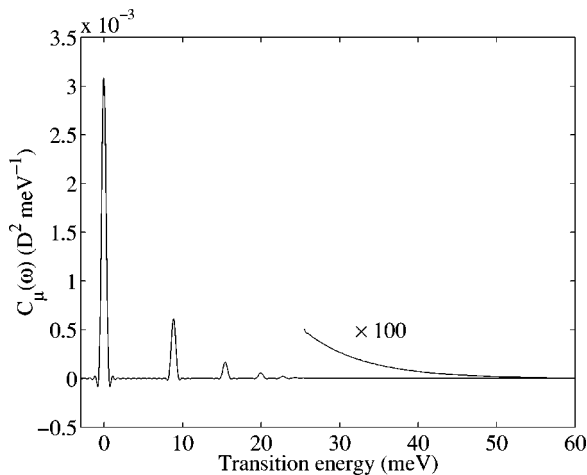


FIG. 5. Calculated dipole moment spectral function  $C_{\mu_p}(\omega)$  for  $\text{H}_2$  on  $\text{Cu}(100)$ . The peaks in the main figure are located at transition energies between the ground state and the bound states. The area of a peak is given by the transition dipole moment intensity while its width and height are given by the energy resolution as determined by the time of wave packet propagation in calculating  $C_{\mu_p}(t)$ . The intensity for energies larger than  $D=25.5$  meV, corresponding to transitions to continuum levels, is magnified by a factor of 100.

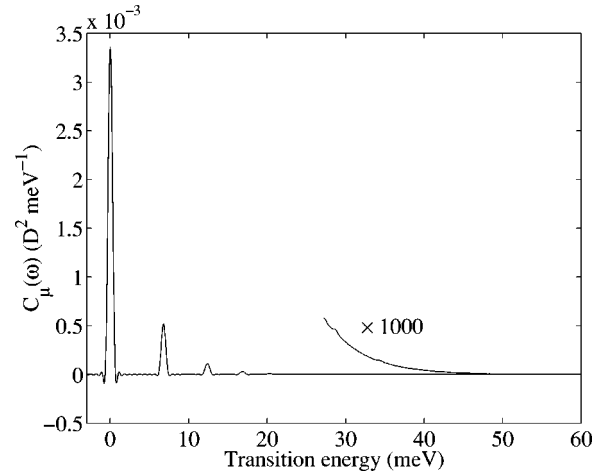


FIG. 6. Calculated dipole moment spectral function  $C_{\mu_p}(\omega)$  for  $\text{D}_2$  on  $\text{Cu}(100)$ . The peaks in the main figure are located at transition energies between the ground state and the bound states. The intensity for energies larger than  $D=27.1$  meV, corresponding to transitions to continuum levels, is magnified by a factor of 1000.

gimes corresponding to transitions to bound and continuum states, respectively, and separated by the binding energy  $D = -E_0$ . For  $\hbar\omega < D$ , the spectra consist of isolated peaks, each located at the energy for a transition between the ground state  $|0\rangle$  and a bound state  $|n\rangle$ , and with the dipole intensity  $|\langle n|\mu_p|0\rangle|^2$  given by the peak area. For energies larger than  $D$ , each spectrum, shown magnified in the inset, instead consists of a continuum of transitions to unbound states. These continuum spectra are weak, and we find that the square root of the integrated intensities are 0.006 D and 0.002 D for  $\text{H}_2$  and  $\text{D}_2$ , respectively. The spectra directly indicate the possibility of dipole excitation resulting in desorption. A common feature of the spectra is that the dipole intensity decreases more rapidly for  $\text{D}_2$  than for  $\text{H}_2$  with increasing transition energy. This isotope effect derives from the fact that the wave functions for the heavier molecule are more localized, which results in smaller wave-function overlaps. The isotope effect is most pronounced for transitions to the continuum states.

From the dipole spectral function for HD, shown in Fig. 7, we also find that rotational transitions are dipole active in agreement with the experimental observations. This is most clearly demonstrated by the peak at 10.3 meV, which derives from the  $j=0 \rightarrow 1$  rotational transition. This dipole-excited rotational transition is observed at 9.9 meV in the HD spectrum in Fig. 2(c). The observed peak is actually the substate  $(j,m)=(1,0)$  excitation, which as discussed below is shifted to lower energy due to the rotational anisotropy. Higher-order rotational transitions and combined rotational-vibrational transitions have energies larger than  $D = 26.4$  meV. Such transitions result in resonant peaks superimposed on the continuum of transitions to translational unbound states, and the oscillatory structure in the spectrum in the inset of Fig. 7 derives from such resonances. For instance, the peak at 33 meV derives from the  $j=0 \rightarrow 2$  rotational transition. These results are not unexpected for HD because of the coupling between rotational and vibrational

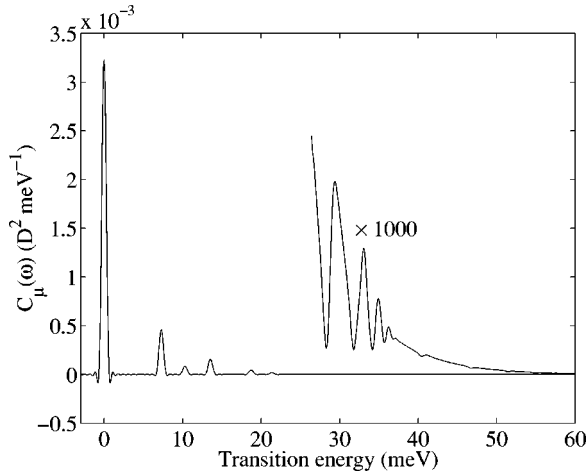


FIG. 7. Calculated dipole moment spectral function  $C_{\mu_p}(\omega)$  for HD on Cu(100). The peaks in the main figure are located at transition energies between the ground state and the bound states. The intensity for energies larger than  $D=26.4$  meV, corresponding to transitions to vibrational continuum levels, is magnified by a factor of 1000. Due to the intrinsic widths of the resonances in the continuum, these peaks are broader than the peaks for transitions to bound states.

motion for this molecule. The good agreement between the calculated and the measured dipole moment also for the transition with predominant  $j=0 \rightarrow 1$  character, as shown in Table I, gives additional support for our dipole moment function. In the calculations for HD, we find that the rotational anisotropy of the potential  $V_2$  has a substantial influence on both dipole moment matrix elements and rotational energy levels. For instance, the matrix element and the energy for the  $j=0 \rightarrow 1$  transition changes from 0.007 to 0.005 D and from 10.3 to 11.2 meV, respectively, when this anisotropy is neglected. For the homonuclear molecules  $H_2$  and  $D_2$ , we find that the rotational anisotropy of the potential does not influence the results for vibrational transition matrix elements and does not result in dipole activity of rotational transitions.

In general, overtone intensities are caused by a nonlinear dependence of  $\mu_p$  with  $z$ , and by the anharmonicities of the potential. These two contributions are often referred to as electrical and mechanical anharmonicities, respectively. We find that the contribution from electrical anharmonicity dominates. This is demonstrated in Table I, where the overtone intensities for  $H_2$ , calculated using a linear dipole function, are shown to be much smaller than those obtained with the exponential dipole function. One minor effect of the mechanical anharmonicity is that the ground-state wave function is centered slightly outside the potential minimum. This explains why the ground-state expectation values of the dipole moment is smaller than  $\mu_p(z_0) = \mu_0$ , as shown in Tables I and II. The effect is larger for  $H_2$  than for  $D_2$ , because its smaller mass makes its wave function less localized in the potential well.

For  $H_2$  adsorbed on the terraces of Cu(510), the dipole intensities decrease more slowly with the transition energy than for the Cu(100) surface, as shown from the calculated

and measured matrix elements in Table II. The larger overtone intensities for  $H_2$  adsorbed on the terraces than on the flat surface are caused by its larger electrical anharmonicity, that is, a larger value of  $\beta$  for  $H_2$  on the terraces than on the flat surface. From these results for the dipole activity, we expect the direct photodesorption rate to be higher from the terraces than from the flat Cu(100) surface.

In a previous analysis of the measured dipole moment matrix elements for hydrogen molecules on Cu(100),<sup>29</sup> the dipole moment was assumed to originate predominantly from the electronic polarization associated with the asymptotic van der Waals interaction:  $\mu_p \propto (z - z_{\text{ref}})^{-4}$ , where  $z_{\text{ref}}$  defines a reference plane.<sup>34,35</sup> In this model, all parameters were calculated from known substrate and molecular electronic properties. Matrix elements were calculated by making a Taylor expansion of the dipole moment from the equilibrium position of the molecule in the ground state and, as shown in Table I, the calculated matrix elements were about the same order of magnitude as the measured values. However, such an expansion can only be used to estimate matrix elements for transitions to the low-lying states, and we find that this model is not appropriate for calculating the direct desorption rate.

## B. Photodesorption

Our calculated dipole intensities for transitions to continuum states are relatively small, indicating that direct photodesorption is a weak process. We find that the rates of desorption, induced by room-temperature blackbody radiation, are  $1.6 \times 10^{-4}$  and  $1.2 \times 10^{-5} \text{ s}^{-1}$  for  $H_2$  and  $D_2$ , respectively, adsorbed on Cu(100). Thus the mean time required to photodesorb an  $H_2$  molecule is about 1.5 h and an order of magnitude longer for  $D_2$ . It is not at all obvious that such a weak process gives effects that are observable in experiments. However, we find from Eq. (19) that due to the direct photodesorption, a  $H_2$  background pressure,  $p_b$ , of about  $10^{-9}$  Torr is required to maintain full coverage of a Cu(100) surface in an ultrahigh-vacuum chamber at room temperature (296 K). This estimated  $H_2$  pressure is in good agreement with the experimental observations reported in Sec. III.

We find that desorption induced by an indirect phonon process that involves excitations of substrate phonons as an intermediate step is negligible in comparison to the direct process. Our evaluation of this rate is based on the expression in Eq. (24), and is determined by the screened charge of the substrate ions  $e^*$  and the maximum longitudinal phonon frequency normal to the surface,  $\omega_{\text{max}}$ .<sup>36</sup> In the case of a Cu(100) surface, previous studies of the surface dipole activity of substrate phonons in Ref. 19 revealed that a good description is obtained with  $e^* = 0.015e$ . The phonon structure is also well known for Cu, and  $\hbar \omega_{\text{max}}$  was determined to be 30 meV in the [100]-direction.<sup>19,38</sup> With these parameter values and in the presence of 296-K blackbody radiation, we obtain desorption rates of about  $5 \times 10^{-8}$  and  $6 \times 10^{-9} \text{ s}^{-1}$  for  $H_2$  and  $D_2$ , respectively. These rates are several orders of magnitude smaller than the direct rates, and we conclude that the direct process is dominating the photodesorption of hy-

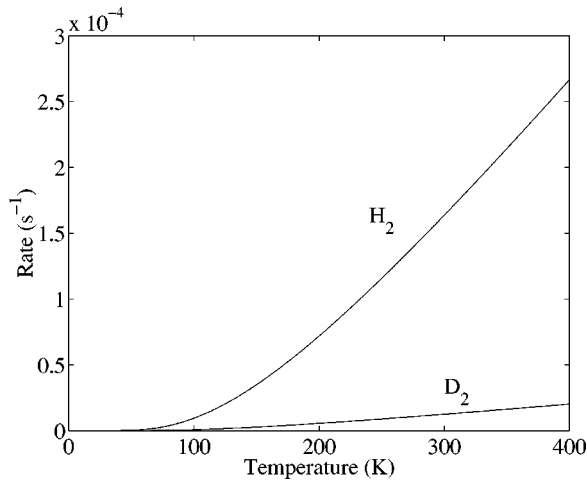


FIG. 8. Calculated direct photodesorption rate for  $\text{H}_2$  and  $\text{D}_2$  physisorbed on  $\text{Cu}(100)$ , as a function of the blackbody radiation temperature.

drogen molecules from  $\text{Cu}(100)$ . The results are also valid for the  $\text{Cu}(510)$  surface, since our EELS experiments show that the dipole activity for this surface is similar to  $\text{Cu}(100)$ .

In order to compare with the experiments described in Sec. III and to identify some characteristic features of the direct photodesorption, induced by blackbody radiation, we have calculated the rate as a function of the radiation temperature. In Figs. 8 and 9, we show the calculated temperature dependencies of the rates for  $\text{H}_2$  and  $\text{D}_2$  desorbing from  $\text{Cu}(100)$  and from the terraces of  $\text{Cu}(510)$ , respectively. The temperature dependence of the rate is determined by the Bose-Einstein photon distribution function and is similar in all cases. At low temperatures,  $k_B T \ll D$ , the rate is Arrhenius-like,  $W_d \propto \exp(-D/k_B T)$ , and at high temperatures  $k_B T \gg D$ , it is approximately linear in temperature:  $W_d \propto T$ . For each surface, the isotope effect of the dipole intensities has a pronounced effect on the desorption rate; the rate is

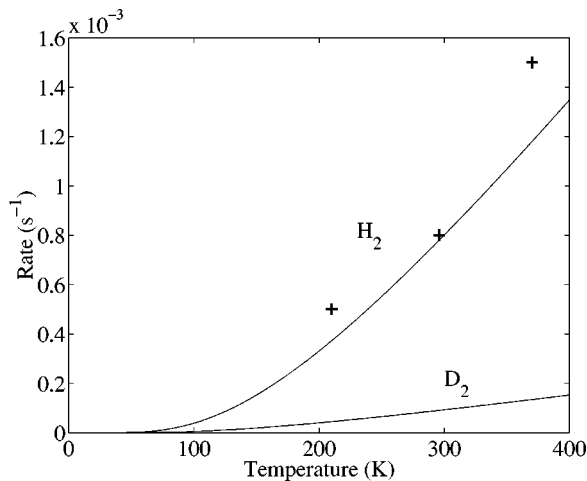


FIG. 9. Calculated direct photodesorption rate for  $\text{H}_2$  and  $\text{D}_2$  physisorbed on the terraces of  $\text{Cu}(510)$ , as a function of the blackbody radiation temperature. The crosses are experimental values for  $\text{H}_2$ , taken from Ref. 11.

about an order of magnitude larger for  $\text{H}_2$  than for  $\text{D}_2$ . The stronger overtone dipole intensity for molecules on the terraces of  $\text{Cu}(510)$  than on  $\text{Cu}(100)$ , results in a larger desorption rate.

Experimentally, we found that background pressures of order  $10^{-9}$  Torr were required to maintain a fixed  $\text{H}_2$  coverage, in agreement with our estimation for the direct photodesorption process. From the terraces, the molecules were observed to desorb with rates  $5 \times 10^{-4}$ ,  $8 \times 10^{-4}$ , and  $15 \times 10^{-4} \text{ s}^{-1}$  at wall temperatures of 210, 296, and 370 K, respectively. These values are in very good agreement with our calculated direct photodesorption rates, as shown in Fig. 9. For  $\text{D}_2$ , we observed at 296 K that the desorption rate was about an order of magnitude smaller than for  $\text{H}_2$ . This finding is also consistent with our calculations.

Desorption rates were also measured in Ref. 3 from ion gauge and mass spectrometer observations for low coverages of  $\text{H}_2$  and  $\text{D}_2$  on a poorly characterized copper surface. With the chamber at room temperature, the rates were found to be in the order of  $10^{-4} \text{ s}^{-1}$  and  $10^{-5} \text{ s}^{-1}$  for  $\text{H}_2$  and  $\text{D}_2$ , respectively. These values are of the same order of magnitude as our calculated and measured rates of photodesorption, both from the terraces of  $\text{Cu}(510)$  and from  $\text{Cu}(100)$ . In particular, the magnitude of the isotope effect is similar in all cases. The good agreement between our calculated direct photodesorption rates and measured rates strongly indicates that the photodesorption observed in the experiments are the results of direct processes.

A large photodesorption rate at a given photon energy flux can be obtained by using a tunable infrared laser as photon source. The strongest coupling between the field and the dipole moment is obtained with a  $p$ -polarized beam at near grazing incidence, where  $\mathbf{e} \cdot \hat{z}$  is maximized. However, as noted previously, the reflection coefficient,  $R_p$ , tends to -1 at near grazing incidence, thus canceling the normal electric field. From calculations of  $R_p$  as a function of incident angle, given in Ref. 16, we find that the optimal configuration is obtained at an angle of incidence of about  $84^\circ$ . With this arrangement and by tuning the photon energy to just above the binding energy  $D$ , where the dipole intensity is strongest, the efficiency of the laser in desorbing the molecule is maximized. The blackbody radiation, on the other hand, is unpolarized, and has an isotropic angular distribution and an energy distribution that stretches from zero energy to well above the energy region where appreciable dipole-induced desorption occurs. The total energy flux of 296-K blackbody radiation through a surface is about  $50 \text{ mW/cm}^2$  with a total photon flux of about  $4 \times 10^{18} \text{ cm}^{-2} \text{ s}^{-1}$ . With a laser of the same photon flux and operating under optimal configuration, we find that it is possible to obtain a direct photodesorption rate of  $2.5 \times 10^{-3} \text{ s}^{-1}$  for  $\text{H}_2$ , a factor of 16 larger than for the blackbody radiation. The cross section for desorption is, however, still small,  $\sim 10^{-22} \text{ cm}^2$ . This can be compared with results from experiments with desorption induced by laser photo excitation of internal vibrational modes, where cross sections on the order of  $10^{-19} \text{ cm}^2$  have been observed.<sup>37</sup>

The use of a tunable infrared laser should result in some interesting effects in desorption of physisorbed HD. The resonant structure in the continuum part of the dipole intensity spectrum, shown in the inset of Fig. 7, implies that a laser can induce resonant photodesorption of HD. This resonant process should be detectable in experiments.

Finally, we argue that the rate for photodesorption of a hydrogen molecule in the physisorption well should be dominated by the absorption of single photons via a bound-continuum state transition rather than by absorption of multiple photons involving bound-bound-state transitions as intermediate steps. This argument is based on the fact that the relaxation rate of the bound states are several orders of magnitude larger than the absorption rate of photons provided by room-temperature blackbody radiation. As shown in Sec. II B, multiple-photon absorption will only be important if it can substantially change the population of the bound states. The magnitude of this change is governed by the relative magnitude of the relaxation rate of the bound states due to emission and absorption of single phonons and the rate of absorption of single photons, respectively. From our earlier study of the lifetimes of the hydrogen molecule in the bound states of the physisorption well,<sup>17</sup> the relaxation rate due to phonon emission and absorption was found to be about  $10^{11}/\text{s}$ . This rate is 13 orders of magnitude larger than the rate of about  $10^{-2}/\text{s}$  from the ground state to the first excited state by absorption of single photons of room-temperature blackbody radiation that we find from Eq. (11) using the values for the dipole matrix elements in Table I. This results in a population of about  $10^{-13}$  of the first excited state, which is roughly the population at a substrate temperature of a few K and cannot be compensated for by a corresponding change in the bound-continuum transition rate  $W_{dm}^{IR}$  from  $m = 0$  to 1. The relative intensity of the dipole spectral function integrated over frequencies corresponding to bound-continuum transitions is about 0.01, and the remaining factors such as the expectation value for the dipole moment, the Bose-Einstein distribution function for room-temperature blackbody radiation have no strong dependence on the bound state level.

## V. CONCLUDING REMARKS

We have calculated the rate of direct photodesorption for  $\text{H}_2$ ,  $\text{D}_2$ , and HD molecules physisorbed on low-index Cu surfaces by absorption of single photons. Two extreme limits of photon sources have been considered: blackbody radiation and an infrared laser beam. In the direct desorption mechanism, the photon field interacts with the dipole moment associated with the motion of the molecule perpendicular to the surface, and excites the molecule from the vibrational ground state to a continuum state, resulting in desorption. The desorption rate is then determined by the intensity of the continuum part of the dipole spectrum. In the calculations we have used a functional form of the dipole moment that is physically reasonable. This form very well reproduces the measured dipole intensities for transitions among the bound states of  $\text{H}_2$ , HD, and  $\text{D}_2$  in the physisorption well. We also find that our calculated direct photodesorption rates, as a

function of blackbody radiation temperature, agree remarkably well with the measured rates for  $\text{H}_2$  on the terraces of a Cu(510) surface. The strong isotope effect observed in the dipole spectra, with weaker overtone spectra for  $\text{D}_2$  than for  $\text{H}_2$ , resulted in a direct photodesorption rate which is about an order of magnitude smaller for  $\text{D}_2$  than for  $\text{H}_2$ . This result is also consistent with experimental observations. We also find that the photodesorption process involving multiple absorption of photons via bound-bound state transitions are negligible compared to photodesorption via absorption of a single photon.

For HD, we found that the mechanical coupling between vibrational and rotational motions, introduced by the asymmetric position of the center of mass of this molecule, resulted in a substantial dipole activity of rotational transitions. Measured and calculated values of the dipole strength of the  $0 \rightarrow 1$  rotational transition agree remarkably well. Combined rotational-vibrational transitions were found to give rise to a resonant behavior of the dipole intensity spectrum for transitions to continuum states of the physisorption potential. Thus we predict the possibility of inducing resonant photodesorption of physisorbed HD by using a tunable infrared photon source, for example, an infrared laser.

We have also calculated the rate of photodesorption induced by an indirect process, involving the excitation of single substrate phonons, which was previously proposed as a possible mechanism responsible for photodesorption of physisorbed molecules. For our physisorption system, we found, using the measured surface dipole activity of substrate phonons, that the rate of desorption by such a process is smaller than the direct rate by several orders of magnitude. Our experimental and theoretical results strongly suggest that the observed photodesorption is the result of a direct process, and we believe that this process can also be effective for other weakly bound and light adsorbates.

## ACKNOWLEDGMENTS

Support by the former Swedish Research Councils for Natural Science (NFR) and Engineering Sciences (TFR), the Institute of Surface and Interface Science (ISIS), University of California, Irvine, and the National Science Foundation Grant No. DMR-0102887 is gratefully acknowledged.

## APPENDIX A: DETAILS OF THE INDIRECT DESORPTION RATE CALCULATION

Here we derive the expression in Eq. (24) for the rate of indirect desorption of a single molecule on a surface. Explicit results for the lattice response functions of a Cu(100) surface that enter this expression and the expression for the rate of photon absorption by single phonons are also derived. To ease the presentation we have used periodic boundary conditions in the lateral directions along the surface.

The indirect desorption of a single molecule adsorbed on a surface is a second-order process, and is induced by the interaction between the lattice and the radiation field and the interaction between the particle and the lattice. As discussed

in Sec. II C, these two interactions are described by the interaction Hamiltonians

$$\begin{aligned} H_{\text{latt-em}} &= -Ne^*(u_0 - u_1)E_z, \\ H_{p\text{-latt}} &= -u_0V'_0 \end{aligned} \quad (\text{A1})$$

where  $N$  is the number of surface unit cells, and we stress again that  $u_0$  and  $u_1$  are the rigid displacements of the first and second surface layers, respectively. The rate of desorption is then given by second-order perturbation theory as

$$W_{\text{ph}} = \frac{16\pi^2}{\hbar^2 c} I(\mathbf{q}, \boldsymbol{\epsilon}) (\boldsymbol{\epsilon} \cdot \bar{z})^2 C_{V'_0}(\omega) |A_1(\omega) + A_2(\omega)|^2, \quad (\text{A2})$$

where  $A_1$  and  $A_2$  involve intermediate single-phonon states,  $|m_{\text{latt}}\rangle$ :

$$A_1(\omega) = Ne^* \sum_{m_{\text{latt}}} \frac{\langle 0_{\text{latt}} | u_0 - u_1 | m_{\text{latt}} \rangle \langle m_{\text{latt}} | u_0 | 0_{\text{latt}} \rangle}{E_{0_{\text{latt}}} - E_{m_{\text{latt}}} - \hbar\omega - i0^+}, \quad (\text{A3})$$

$$A_2(\omega) = Ne^* \sum_{m_{\text{latt}}} \frac{\langle 0_{\text{latt}} | u_0 | m_{\text{latt}} \rangle \langle m_{\text{latt}} | u_0 - u_1 | 0_{\text{latt}} \rangle}{E_{0_{\text{latt}}} - E_{m_{\text{latt}}} + \hbar\omega + i0^+}. \quad (\text{A4})$$

The functions  $A_1$  and  $A_2$  are, within linear-response theory, related to the response of  $u_0$  to the field  $E_z$  as

$$|A_1(\omega) + A_2(\omega)|^2 = |\eta(\omega)|^2, \quad (\text{A5})$$

where  $\eta(\omega)$  is the response of  $u_0$  to the field  $E_z$ :

$$\eta(\omega) = \frac{u_0(\omega)}{E_z(\omega)}. \quad (\text{A6})$$

This response function and  $\alpha(\omega)$  in Eq. (21) can be calculated by solving a one-dimensional set of coupled equations describing the dynamics of longitudinal phonon propagating normal to the surface. In a nearest-neighboring interlayer force-constant model, the dynamics of the rigid substrate layers is then governed by

$$-M\omega^2 u_0 + M\Omega^2(u_0 - u_1) = e^* E_z, \quad (\text{A7})$$

$$-M\omega^2 u_1 + M\Omega^2(2u_1 - u_0 - u_2) = -e^* E_z, \quad (\text{A8})$$

$$-M\omega^2 u_2 + M\Omega^2(2u_2 - u_1 - u_3) = 0 \quad (\text{A9})$$

⋮

Here  $M$  is the mass of a substrate atom, and  $M\Omega^2$  is the force constant between the lattice planes. The maximum frequency  $\omega_{\text{max}}$  of this phonon branch is given by  $\omega_{\text{max}} = 2\Omega$ . Note that the factor of  $N$  in the total force exerted by the electric field on the rigid substrate layer in Eq. (A1) is canceled by the factor of  $N$  in the total mass and the total force constants for the rigid displacements of the substrate layers. From the homogeneous equations for the bulk layers  $i \geq 2$ ,

we obtain a closed second-order equation for the response function  $\chi(\omega)$ , defined by  $u_{i+1}(\omega) = \chi(\omega)u_i(\omega)$ , and with the solution

$$\chi(\omega) = 1 - 2\bar{\omega}^2 + i2\bar{\omega}\sqrt{1 - \bar{\omega}^2} \quad (\text{A10})$$

for  $0 < \bar{\omega} = \omega/\omega_{\text{max}} < 1$ . Using this result, the inhomogeneous equations for the two surface layers can be solved, and the lattice response functions are given by

$$\eta(\omega) = \frac{4e^*}{M\omega_{\text{max}}^2} \chi(\omega) \quad (\text{A11})$$

and

$$\alpha(\omega) = \frac{4e^{*2}}{M\omega_{\text{max}}^2} (1 + 4\bar{\omega}^2 - 8\bar{\omega}^4 + i8\bar{\omega}^3\sqrt{1 - \bar{\omega}^2}). \quad (\text{A12})$$

## APPENDIX B: DETAILS OF THE WAVE-PACKET PROPAGATION

We have used a pseudospectral method<sup>39</sup> to solve the two dimensional, time-dependent Schrödinger equation in a discrete variable representation (DVR).<sup>40</sup> The spectral basis is a direct product of plane waves,  $e^{ik_z z}$ , in the  $z$  coordinate and Legendre functions,  $P_j(\cos \theta)$ , in the  $\theta$  coordinate. The DVR points in the  $z$  coordinate form a uniform grid, and in the  $\theta$  coordinate the points are Gauss-Legendre quadrature points. The wave function at a time  $t = N\Delta t$  is approximated by the Trotter formula, and the split-operator approximation for the short-time propagator:

$$\begin{aligned} |\psi(N\Delta t)\rangle &\approx \left[ \exp\left(-\frac{i}{2\hbar}V\Delta t\right) \exp\left(-\frac{i}{\hbar}T\Delta t\right) \right. \\ &\quad \left. \times \exp\left(-\frac{i}{2\hbar}V\Delta t\right) \right]^N |\psi(0)\rangle. \end{aligned} \quad (\text{B1})$$

The potential-energy operator  $V$  is a local operator on the real-space grid, and its effect on the wave function can be evaluated directly on this grid. The effect of the kinetic-energy operator  $T$  on the wave function can be evaluated directly after making a transformation to the spectral representation, in which  $T$  is local:

$$\langle k_i j | T | k_i' j' \rangle = \left( \frac{\hbar^2 k_i^2}{2m_p} + E_j \right) \delta_{ii'} \delta_{jj'}. \quad (\text{B2})$$

Here we have used the gas-phase rotational energies of  $\text{H}_2$ ,  $\text{HD}$  and  $\text{D}_2$  for  $E_j$ .<sup>41</sup> Thus the propagation of the wave function proceeds by repeatedly performing transformations between the real-space grid and the spectral grid. In the  $z$  coordinate, the forward and backward transformations are performed efficiently by fast Fourier transforms, whereas in the  $\theta$  coordinate these transformations involve small matrix multiplications. The Fourier method introduces implicitly periodic boundary conditions in the  $z$  direction. Therefore, in order to have a good description of transitions to the con-

tinuum states, we have added a complex absorbing potential<sup>42</sup> at the grid boundary.

Finally, we present some numerical details of the calculations. The window function that we have used in this work is a variant of the Hanning window function.<sup>22</sup> In the DVR, the grid spacing in each coordinate is determined from the maximum kinetic energy of the molecule, which is set to be about 100 meV. In the  $z$  coordinate, the grid spacing is then given by  $\Delta z |k_{\max}| < \pi$ , while the number of grid points in the  $\theta$  coordinate is determined by the maximum rotational quantum number,  $j_{\max}$ , from  $E_{j_{\max}} > E_{\max}$ . In the propagation, the

length of one time step must satisfy  $\Delta t < \pi/E_{\max}$ . To meet these conditions, for H<sub>2</sub> we have chosen  $\Delta z = 0.55a_0$ ,  $j_{\max} = 4$ , and  $\Delta t = 400$  a.u. The absorbing potential starts at a distance  $z = z_{\max} = 40a_0$  from the surface and is given by<sup>42</sup>

$$V_{\text{abs}} = -iAN \exp\left(\frac{2L}{z - z_{\max}}\right), \quad (\text{B3})$$

where  $N = 13.22$  is a constant, while  $A$  and  $L$  are both coefficients related to the energies of the system. In this work we have used  $L = 15$  a.u. and  $A = 1.12E_{\max}$ .

- 
- <sup>1</sup>T. J. Chuang and I. Hussla, Phys. Rev. Lett. **52**, 2045 (1984).  
<sup>2</sup>I. Hussla, H. Seki, T. J. Chuang, Z. W. Gortel, H. J. Kreuzer, and P. Piercy, Phys. Rev. B **32**, 3489 (1985).  
<sup>3</sup>J. N. Chubb, L. Gowland, and I. E. Pollard, J. Phys. D **1**, 361 (1968).  
<sup>4</sup>C. Benvenuti, R. S. Calder, and G. Passardi, J. Vac. Sci. Technol. **13**, 1172 (1976).  
<sup>5</sup>J. Cui, J. S. C. Fain, and W. Liu, J. Vac. Sci. Technol. A **7**, 1850 (1989).  
<sup>6</sup>P. M. Ferm, S. R. Kurtz, K. A. Pearlstine, and G. M. McClelland, Phys. Rev. Lett. **58**, 2602 (1987).  
<sup>7</sup>J. Lin and T. F. George, Chem. Phys. Lett. **66**, 5 (1979).  
<sup>8</sup>C. Jedrzejek, K. F. Freed, S. Efrima, and H. Metiu, Surf. Sci. **109**, 191 (1981).  
<sup>9</sup>K. A. Pearlstine and G. M. McClelland, Surf. Sci. **134**, 389 (1983).  
<sup>10</sup>K. Shiang, Surf. Sci. **292**, 145 (1993).  
<sup>11</sup>M. Hassel, K. Svensson, M. Persson, and S. Andersson, Phys. Rev. Lett. **80**, 2481 (1998).  
<sup>12</sup>S. Andersson and J. Harris, Phys. Rev. Lett. **48**, 545 (1982).  
<sup>13</sup>L. Wilzén, F. Althoff, S. Andersson, and M. Persson, Phys. Rev. B **43**, 7003 (1991).  
<sup>14</sup>S. Andersson, L. Wilzén, and M. Persson, Phys. Rev. B **38**, 2967 (1988).  
<sup>15</sup>J. D. Jackson, *Classical Electrodynamics*, 2nd ed. (Wiley, New York, 1975).  
<sup>16</sup>B. N. J. Persson and A. I. Volokitin, Surf. Sci. **310**, 314 (1994).  
<sup>17</sup>M. Persson, L. Wilzen, and S. Andersson, Phys. Rev. B **42**, 5331 (1990).  
<sup>18</sup>S. Andersson, L. Wilzen, M. Persson, and J. Harris, Phys. Rev. B **40**, 8146 (1989).  
<sup>19</sup>S. Andersson, B. N. J. Persson, M. Persson, and N. D. Lang, Phys. Rev. Lett. **52**, 2073 (1984).  
<sup>20</sup>E. W. Montroll and K. E. Shuler, Adv. Chem. Phys. **1**, 361 (1958).  
<sup>21</sup>M. Persson, J. A. Strosio, and W. Ho, Phys. Scr. **36**, 548 (1987).  
<sup>22</sup>M. D. Feit, J. A. Fleck, Jr., and A. Steiger, J. Comput. Phys. **47**, 412 (1982).  
<sup>23</sup>O. Cipri, R. Baer, and R. Kosloff, Surf. Sci. **351**, 24 (1996).  
<sup>24</sup>P. Nordlander, C. Holmberg, and J. Harris, Surf. Sci. **152**, 702 (1985).  
<sup>25</sup>P. Nordlander, C. Holmberg, and J. Harris, Surf. Sci. **175**, L753 (1986).  
<sup>26</sup>A. Chizmeshya and E. Zaremba, Surf. Sci. **268**, 432 (1992).  
<sup>27</sup>J. Harris and P. J. Feibelman, Surf. Sci. **115**, L133 (1982).  
<sup>28</sup>S. Andersson in *Vibrations at Surfaces*, edited by R. Caudano, J. M. Gilles, and A. A. Lucas (Plenum, New York, 1982) p. 169; K. Svensson, Ph.D. thesis, Department of Applied Physics, Chalmers University of Technology and Göteborg University, Göteborg, Sweden, 1997.  
<sup>29</sup>K. Svensson and S. Andersson, Phys. Rev. Lett. **78**, 2016 (1997).  
<sup>30</sup>Measured at sufficiently high energy resolution, the H<sub>2</sub>-Cu(100) spectrum reveals a weak ( $j, m$ ) substate splitting with (2,0) at 43.7 meV and (2, ±2) at 45.1 meV; see Ref. 31.  
<sup>31</sup>K. Svensson and S. Andersson, Surf. Sci. **392**, L40 (1997).  
<sup>32</sup>L. Bengtsson, K. Svensson, M. Hassel, J. Bellman, M. Persson, and S. Andersson, Phys. Rev. B **61**, 16 921 (2000).  
<sup>33</sup>M. Gruyters and K. Jacobi, Chem. Phys. Lett. **225**, 309 (1994).  
<sup>34</sup>P. R. Antoniewicz, Phys. Rev. Lett. **32**, 1424 (1974).  
<sup>35</sup>E. Zaremba, Phys. Lett. **57A**, 156 (1976).  
<sup>36</sup>The negligible rate for indirect desorption compared to direct desorption can be understood from the small probability of absorption of photons by longitudinal phonons in the surface region and the small cross section for such phonons to desorb a physisorbed hydrogen molecule. For instance, with a  $\hbar\omega = 25.5$  meV laser under an optimal configuration, we find that the probability for a photon to excite a phonon is  $P_{\text{abs}}(\mathbf{q}, \epsilon) \approx 2.5 \times 10^{-7}$  and the cross section for such a phonon to desorb a molecule is  $\sigma_{\text{ph}}(\omega) \approx 2.4 \times 10^{-3} A_{\text{sc}}$  where  $A_{\text{sc}} = 6.5 \text{ \AA}^2$  is the area of the surface unit cell. Thus the total desorption cross section for such a real phonon process is about  $6 \times 10^{-10} A_{\text{sc}}$ . We find that the process involving virtual phonons contributes with a desorption cross section of less than  $2 \times 10^{-10} A_{\text{sc}}$  in this case.  
<sup>37</sup>T. J. Chuang, Surf. Sci. Rep. **3**, 1 (1983).  
<sup>38</sup>E. C. Svensson, B. N. Brockhouse, and J. M. Rowe, Phys. Rev. **155**, 619 (1966).  
<sup>39</sup>R. Kosloff, in *Time-Dependent Quantum Molecular Dynamics*, edited by J. Broeckhove and L. Lathouwers (Plenum Press, New York, 1992), pp. 97–116.  
<sup>40</sup>J. C. Light, in *Time-Dependent Quantum Molecular Dynamics* (Ref. 39), pp. 185–199.  
<sup>41</sup>U. Harten, J. P. Toennies, and C. Wöll, J. Chem. Phys. **85**, 2249 (1986).  
<sup>42</sup>G. G. Balint-Kurti and A. Vibók, in *Numerical Grid Methods and Their Application to Schrödinger's Equation*, edited by C. Cerjan (Kluwer, Dordrecht, 1993), pp. 195–205.